crystals

MDPI

Review

Recent Progress on High-Entropy Films Deposited by Magnetron Sputtering

Mohamed El Garah [1,2,*], Pascal Briois [3] and Frederic Sanchette [1,2]

[1] LASMIS—Laboratoire des Systèmes Mécaniques et d'Ingénierie Simultanée, Antenne de Nogent-52, Pôle Technologique de Sud-Champagne, 52800 Nogent, France; frederic.sanchette@utt.fr
[2] LRC CEA-LASMIS, Nogent International Center for CVD Innovation (NICCI), Antenne de Nogent, Pôle Technologique de Haute Champagne, 52800 Nogent, France
[3] Institut FEMTO-ST, FCLAB, UMR 6174, CNRS, University Bourgogne Franche-Comté, 15B Avenue des Montboucons, 25030 Besançon, France; pascal.briois@utbm.fr
* Correspondence: mohamed.el_garah@utt.fr

Abstract: High-entropy films (HEFs) are of considerable interest in surface engineering applications due to their superior properties, such as good corrosion resistance, good thermal stability and excellent high temperature oxidation. Recently, the scientific community has seen an increasing development of the multicomponent coatings, improving their properties compared to conventional films. Technically, different strategies have been exploited to fabricate HEFs. Magnetron-sputtered HEFs have made significant advancements in this field. HEFs have various applications given their interesting performances. This article overviews the development and the outcome of HEFs prepared using the magnetron sputtering technique. The classification of HEFs is reported. The effect of magnetron sputtering parameters on the microstructural, mechanical, electrochemical and thermal properties of HEFs is also discussed. Applications of HEFs are reported in the last section.

Keywords: high-entropy films; magnetron sputtering; PVD; corrosion; thermal stability

check for updates

Citation: El Garah, M.; Briois, P.; Sanchette, F. Recent Progress on High-Entropy Films Deposited by Magnetron Sputtering. *Crystals* **2022**, *12*, 335. https://doi.org/10.3390/cryst12030335

Academic Editors: Rui Feng, Ke An, Peter K. Liaw and Hongbin Bei

Received: 18 January 2022
Accepted: 23 February 2022
Published: 27 February 2022

Publisher's Note: MDPI stays neutral with regard to jurisdictional claims in published maps and institutional affiliations.

Copyright: © 2022 by the authors. Licensee MDPI, Basel, Switzerland. This article is an open access article distributed under the terms and conditions of the Creative Commons Attribution (CC BY) license (https://creativecommons.org/licenses/by/4.0/).

1. Introduction

The surface is a key factor to be considered in the development of materials with high performance. Coating the materials with films with superior properties allows the replacement of low-quality alloys with materials that can meet extreme requirements. The quality of a surface has a great impact on the material's durability. Various coatings have been developed to combat different causes of degradation. High-temperature oxidation, wear effect and corrosive environments are all important factors that affect the durability and the performances of the coatings.

Compared to conventional alloys, coatings are of considerable interest in the field of materials development. Since 2004, a new approach was reported that involved developing high-entropy alloys (HEAs), which can be an alternative solution to improve the physical and the chemical properties of multi-element alloys. HEAs are defined as an alloy of at least five elements with an atomic percentage varying from 5 at.% to 35 at.%. Since their invention, several names have been reported in the literature, such as complex concentrated alloys [1], multi-principal element alloys [2], multi-component alloys [3] and compositionally complex alloys [4]. In addition, four characteristic effects are reported and known for HEAs: high entropy, severe lattice distortion, slow diffusion and the cocktail effect. All the cores effect are reported and explained in detail by Yeh et al. in reference [5]. Combining the four effects leads to HEAs with interesting physical and chemical properties. Three different structures of HEAs—amorphous, intermetallic compounds or solid solutions—have been reported. The solid solution is either face-centered cubic (fcc), body-centered cubic (bcc) or hexagonal close-packed (hcp). Moreover, intensive research always focuses on the development of coatings with excellent properties,

such as high hardness, good wear resistance [6], outstanding thermal stability [7] and excellent oxidation and corrosion resistance [8,9]. Due to those promising properties, HEFs show great potential for engineering fields, such as aerospace materials [10], catalysts [11], metallurgical materials [12] and materials for nuclear applications [13].

Developing surface coatings is an effective strategy to improve the durability of materials by enhancing their functional properties. Many investigations have been focused on the development of coatings with improved performance on low-cost materials. Hard conventional coatings, such as nitrides and carbides of transition metal, have shown their potential for improving hardness and wear resistance [14,15]. However, these traditional binary or ternary nitrides and carbides cannot satisfy the growing demand. For example, TiAlN shows good oxidation resistance, but its resistance is well below than that of HEFs (AlCrNbSiYTi)N [16]. Kretschmer et al. showed also the improved oxidation resistance of (AlCrNbTaTi)N at 850 °C for 100 h [17]. High-entropy nitrides and carbides form simple solid solutions exhibiting better mechanical properties due to the strong covalent bonds between the elements and the large strain mismatch. Other investigations are concerned with high-entropy oxides due to their special properties. For example, $(AlCrTaTiZr)O_x$ maintains its amorphous structure after annealing at 800 °C for 1 h, and its hardness and Young's modulus are 20 GPa and 260 GPa, respectively [18]. $(AlCrNbTaTi)O_2$ showed its ability to maintain single-phase crystalline with rutile structure after vacuum annealing at 1200 °C [19]. The studies of high-entropy oxides are still limited, and further investigations are needed to explore the influence of oxygen content on their performances. HEFs are under extensive study due to their superior structural properties (multi-element solid solutions) and excellent mechanical and tribological performances. Various HEFs have been deposited by magnetron sputtering, revealing superior properties [17,20–23] compared to the conventional coatings. Using the magnetron sputtering technique, a series of deposition parameters have been used to control the microstructure of HEFs. The parameters include gas flow rate [13,21,24–26], substrate temperature and pressure [27,28], as well as the bias voltage [29,30]. The entropy is the launch pad for the future exploration of new materials to be exploited in different fields.

Three categories of HEF are mainly reported: (i) Metallic films formed with transition metals, such as Al, Co, Cu, Cr, Ni, Ti, V and Mn. Metallic refractory HEFs are based on elements with high melting temperatures, such as Hf, Zr, Cr, Ta, W or Mo. Such HEFs have excellent corrosion and high-temperature oxidation resistance. (ii) Ceramic films that are mainly composed of transition metal elements mixed with nitrogen, carbon, oxygen or boron. Among these materials, nitrides are much harder compared to metallic compounds. (iii) Composite films that are presented as a matrix/reinforcement. Tian et al. [31] added Ni60 as a reinforcement to an AlCoCrFeNiTi coating, that is, as the matrix, to enhance its mechanical and tribological properties. AlCoCrFeNiTi/Ni60 was prepared by plasma spraying, and the results showed an improved hardness and wear resistance at high temperatures [31].

Review articles have been recently reported on HEFs, including the preparation methods, properties and applications. Li et al. [32] discussed the relationships between the microstructures and the properties of coatings obtained by different methods. Sharma's review paper [33] focused on the development of HEA materials as coating for demanding and high-performance protection in extreme conditions. Duchaniya et al. [34] reported on the concept, classes, preparation, properties and applications of HEA coatings. Fabricating HEFs by using magnetron sputtering is advantageous. Desired stoichiometric films can easily be obtained, and the quenching rate is high (10^9 K/s), which favors the synthesis of supersaturated solid solutions. The present review gathers recent works on HEFs prepared using magnetron sputtering techniques by focusing on the deposition parameters' effect on their properties and performances. This includes the evolution of their structural, mechanical, tribological and electrochemical properties as a function of various factors. The oxidation resistance and thermal stability of HEFs are discussed. Therefore, a brief discussion of the effect of the configurational entropy is provided. No explicit

investigations are performed in the case of HEFs, as the intention is to report on the latest developments. The review is presented in five sections. Section 1 introduces high-entropy alloys. Section 2 gives details on the process of magnetron sputtering deposition techniques for HEFs. Section 3 deals with the mechanical, tribological, electrochemical and physical properties of HEFs prepared by magnetron sputtering. Section 4 covers the different applications of HEFs. Finally, Section 5 summarizes the challenging development of HEFs and gives future recommendations.

2. High-Entropy Films Deposited by Magnetron Sputtering

Several HEF compositions have been reported to be competitive against the conventional alloys. These films are born of a strong need to develop new protective coatings for operating under extreme conditions. Various investigations and results have been reported since the invention of these HEFs. Figure 1 shows the number of research articles published on HEFs prepared using the magnetron sputtering technique in peer-reviewed journals since 2006. The citation number is included based on Scopus data. Figure 2 provides an overview of the different elements used for developing HEFs with magnetron sputtering. Al and Cr have been widely used in the various compositions. Many investigations have been performed to improve the film performance, such as the oxidation resistance of refractory alloys, through the addition of elements, including Al and Cr [35,36]. These elements allow the formation oxide layers (Al_2O_3, Cr_2O_3) that act as protective coatings.

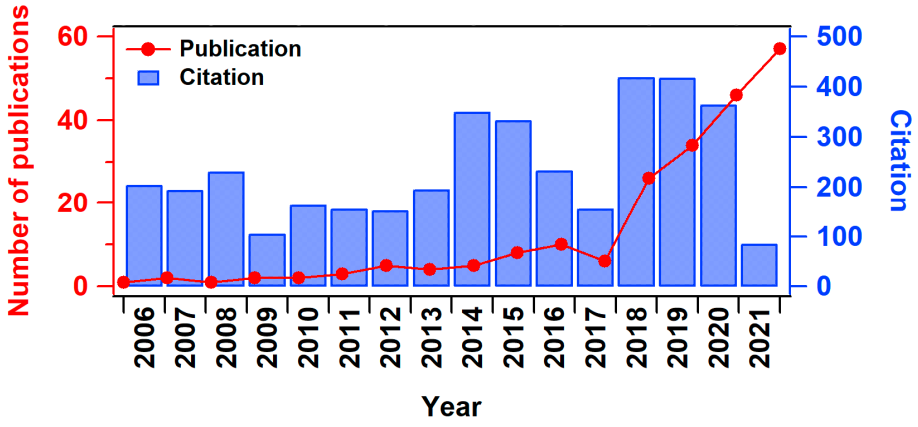

Figure 1. Number of reported publications on magnetron-sputtered HEFs. The histogram shows the number of the articles from 2006 to December 2021. The red curve displays the citation number of the articles per year. The results are plotted according to statistical analysis from the Scopus website.

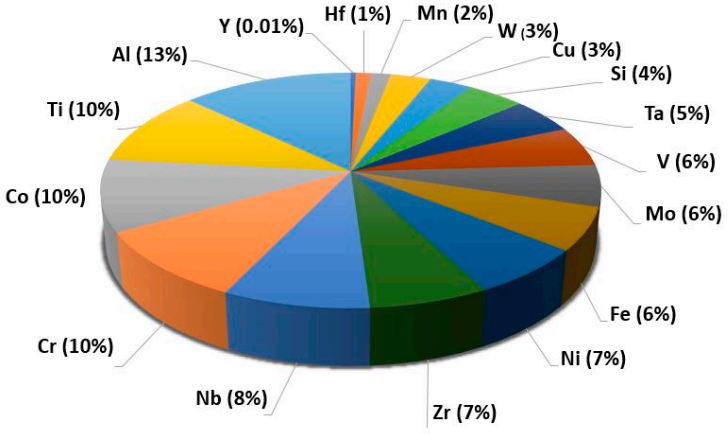

Figure 2. Selected elements used as feedstock for HEFs deposited by magnetron sputtering.

Before discussing the relation between the magnetron parameters and HEF properties, the configurational entropy ΔS_{conf} contribution to the Gibbs energy needs to be mentioned. The high configurational entropy, which is supposed to be the dominant term of the free energy, can lead to a decrease in the Gibbs energy, favoring the formation of solid solutions rather than intermetallic compounds. The effect of the configurational entropy ΔS_{conf} has been reported in the literature, but for very limited studies, and was only mentioned in the case of bulk HEAs [37,38]. Otto et al. reported that maximizing the configurational entropy cannot be a sufficient condition in which to form the solid solution. When starting from CoCrFeMnNi and adding other elements, a single phase was not obtained [38]. Laurent-Brocq et al. [39] compared high-entropy alloys and conventional diluted multielement alloys by examining $Co_xCr_xFe_xMn_xNi_{100-x}$, with x varying from 2 to 25%. The study showed that the diluted alloys exhibit a single solid solution, while some of the concentrated alloys present several phases.

In the case of HEFs, and to the best of our knowledge, no study has explicitly reported on that aspect. We have conducted a survey on the literature relating to AlCrTaTiZr [40] and AlCrTaTiZrMo films [41], which have been coated by RF magnetron sputtering. The equimolar compositions of these films have different configurational entropies. Both films present amorphous structures, but have different mechanical properties. The hardness and Young's modulus of AlCrTaTiZr are 9.3 GPa and 140 GPa, and of AlCrTaTiZrMo are 11.2 and 193 GPa. On the other hand, Braeckman et al. examined the influence of two different (Ge or In) solute elements on the phase formation of CoCrCuFeNi films [42]. They reported that if the solutes exceed a certain threshold, then the crystalline solid solution is not stable, and an amorphous structure is favored. As regards the four core effects of HEAs/HEFs, given that there are very limited reports on the effect of ΔS_{conf} on their properties, more efforts are required in this field to clarify this issue.

3. Process

3.1. Deposition of HEFs

Conventionally, most films are based on one or two principal elements. Their development consists of selecting the principal element and adding minor elements, sometimes in large numbers, to improve their physical, chemical and mechanical properties. Standard physical vapor deposition (PVD) films, such as Ni-superalloys, Al, Ti and Cu, have been investigated and reported on. Standard nitrides films present interesting properties compared to ordinary materials. For example, TiN and TiAlN present oxidation temperatures around 700 °C and 900 °C, respectively [16]. Other similar films show a good corrosion resistance, such as ZrN [43–46], making them potential coatings for various applications.

Compared to these, various HEFs have recently been produced showing superior properties, as mentioned above. For example, HEF nitrides, as a function of the nitrogen flow rate, are reported to be potential candidates for replacing Ni superalloys. It was found that the constituting elements strongly affect their microstructures and, consequently, their properties. The microstructure of HEFs can be the subject of the four core effects. These characteristics are not present in the case of standard PVD films, highlighting the importance of developing new films with better performances. The (AlCrNbSiTi)N HEF investigated by Shen et al. [16] has a superior oxidation temperature compared to the standard ones (TiN, TiAlN). (AlCrNbSiTi)N has an oxidation temperature of around 1100 °C. In addition, the amorphous structure can be more anti-corrosive due to its lack of boundaries. However, the formation of solid solutions which are highly favored in various HEFs can improve the corrosion resistance of the materials [47,48]. Therefore, HEFs have the potential to possess superior performance compared to standard PVD films and can be used under extreme conditions.

Basically, two methods can be used to prepare the HEFs: the sputtering of all elements from one composite target or the co-sputtering of pure elemental targets. It is possible to use an HEA target that enables the good control of the stoichiometry of different elements, as long as target composition is conserved. HEFs can be deposited by co-sputtering the

pure metallic targets, and the film composition is adjusted with each discharge power. A reactive sputtering mode can be implemented by introducing reactive gases (N_2, CH_4, C_2H_2 or O_2) in the vacuum chamber in order to synthetize nitrides (HENF; known as High-Entropy superlattice Nitride Films [49,50]), carbides (HECF) or oxides (HEOF).

3.2. DC Magnetron Sputtering

The basic sputtering process has been known for many years, and several coating materials have been deposited with this technique. In this process, a cathode is bombarded by energetic ions generated in a plasma. The bombardment process results in sputtering, whereby atoms of the target can condense onto the substrate [51–53]. The process is carried out in a closed chamber pumped to a low pressure before the deposition. However, the basic process is limited by several effects, such as a low deposition rate, a low ionization coefficient in the plasma and the heating effect of the substrate. Magnetron sputtering has been developed to overcome these limitations [54]. Magnetrons use a magnetic field parallel to the target surface that can constrain the movement of secondary electrons near the target. Magnets are positioned at the central axis with an opposite orientation to generate rings of magnets between the edge and the center of the target. This was developed to trap electrons close to the target and increase the probability of ionizing collisions between electrons and atoms. The increased ionization results in the formation of a dense plasma near the target. The ion bombardment of the target in this case results in a higher sputtering rate and the deposition rate increases. In addition, the high ionization in this magnetron mode means that the discharge can be kept at low operating pressures compared to the basic mode.

3.3. HiPIMS

High Power Impulse Magnetron Sputtering (HiPIMS) technology [55] allows the user to generate very high instantaneous currents while keeping the target at low temperatures through the use of short pulses (from a few microseconds to a few hundred microseconds). The short pulses make it possible to maintain the discharge by avoiding the creation of unwanted arcs if the duration of the pulses is sufficiently reduced (less than 50 ms). In the case of long pulses, the power supplies are often coupled to an arc suppressor. HiPIMS, which leads to highly ionized discharges, has a number of advantages. For example, the use of a high voltage produces highly energetic ions. This often results in denser films compared to those produced by conventional techniques. The energetic metal ions allow the layer to be compact during the film's growth, either via a transfer of momentum to the atoms of the growing film, or by allowing an increased diffusion of the metal ion atoms on the surface. Moreover, ion etching before the deposition step allows the optimization of the interface for a better adhesion.

Few investigations have been reported in the literature on the study of HEFs using HiPIMS [56–58]. Xu et al. investigated the nitrogen effect on the microstructure and mechanical properties of AlCrTiVZr HEFs [57]. The metallic element contents and the deposition rate decreased as the nitrogen flow increased, which was associated with the target poisoning. An amorphous structure was formed at low nitrogen levels (<4 sccm) and a single-phased fcc solid solution appeared after increasing the nitrogen level more than 4 sccm. The hardness was measured at 41.8 GPa, which meant that this film could be classified as a super-hard material compared to other HEFs. This may be due to the densification of the film using the HiPIMs process. The same group reported the synthesis of another HEF (AlCrTiVZrN) deposited by HiPIMS and a DC magnetron sputtering (DCMS) process. They revealed that the film exhibits a denser microstructure than that obtained via DCMS (Figure 3) [56]. Bachani et al. reported also that a (TiZrNbTFe)N film containing 32 at.% nitrogen has a very dense microstructure [58]. The hardness was measured at 36.2 GPa. This shows how the densification of the films affects their mechanical properties. In addition, the same film has excellent corrosion resistance compared to others obtained with different nitrogen content, essentially because of the compact morphology [58].

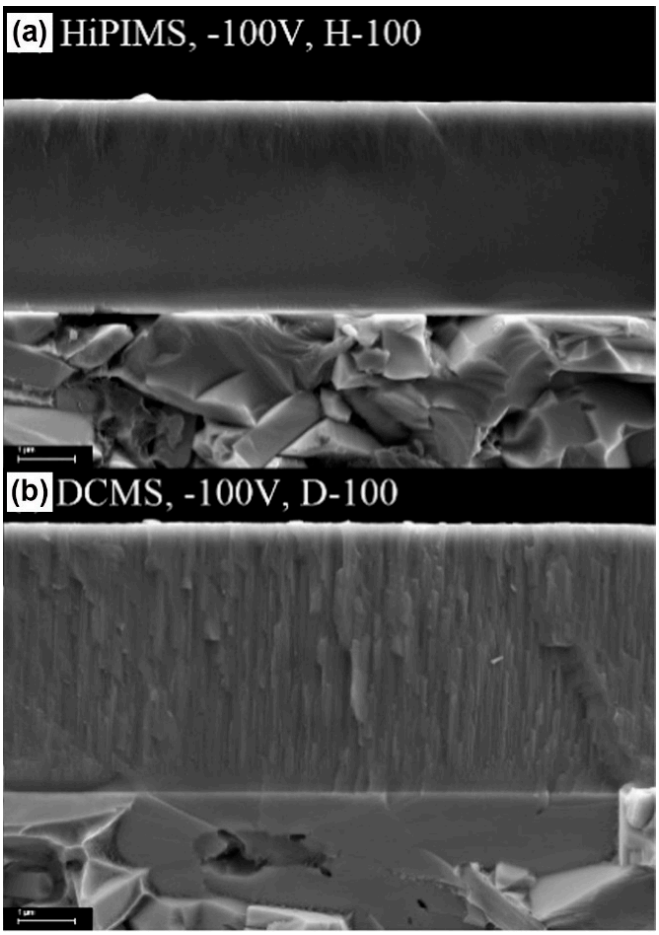

Figure 3. Cross-sectional morphology of (**a**) HiPIMS-deposited and (**b**) DC magnetron sputtering-deposited (AlCrTiVZr)N films. Figure reproduced and modified with permission of ref. [56]. Copyright 2021 Applied Surface Science.

3.4. Deposition Rate

The deposition rate of HEFs prepared via magnetron sputtering was found to be influenced by various parameters, such as substrate temperature, substrate bias, working pressure and reactive gas flow rate (N_2, CH_4/C_2H_2, O_2). Shen et al. studied $(Al_{1.5}CrNb_{0.5}Si_{0.5}Ti)_{50}N_{50}$ nitrides by changing the substrate bias [29]. The deposition rate decreased by 20% when the bias was varied from 0–200 V, which reflects an increase in the re-sputtering phenomenon, even in a weakly ionized discharge. Gas flows such as N_2, CH_4/C_2H_2 and O_2 were also found to decrease the deposition rate of the films. During the preparation of HEFs, the introduction of the gas led to the formation of nitrides, carbides and oxides resulting from target poisoning [20,21,25,26,59,60]. Chang et al. have shown that a deceasing deposition rate occurs with an increase in the substrate temperature (rapid decreasing was observed for temperatures above 300 °C). The decrease is due to the evaporation of the film elements at high temperatures [61]. The pressure was also found to influence the properties of HEFs [27]. As reported by Kim et al., the deposition rate of the AlCoCrNi decreases as the pressure changes from 1.33×10^{-1} to 1.33 Pa. Thus, by increasing the pressure, the collision between the atoms emitted from the target and gases increases in the vacuum chamber. The collision influences the average path of different elements of HEFs and slows down their arrival at the substrate surface. This is a known phenomenon for conventional alloys, but in the case of HEFs, the effect is important because of the presence of several elements. This effect is due to the decrease in the free path of emitted atoms from the target because of their collision with gases in the chamber.

4. Properties of HEFs Deposited by Magnetron Sputtering

4.1. Morphology and Structure

4.1.1. Morphology

Most reported HEFs, prepared via magnetron sputtering, are characterized by columnar, dense, dendrite-like and fibrous-like morphology. The change of the morphology has been reported to be influenced by the deposition parameters, such as substrate bias, substrate temperature, pressure and reactive gases. The densification of the films is due to the high mobility of adatoms on the substrate surface.

Morphologically, HEFs can be controlled by varying many sputtering parameters. A columnar structure is formed with a bias ranging from −50 V to −100 V, while very fine striation lines with spacing were observed on AlCrTiWNbTa films at −150 V [62]. Yu et al. reported three morphologies of a CrNbSiTiZr film: a columnar shape is obtained at 0 V, it moves between columnar and fine fibers at −50 V and becomes compact at −200 V [63]. The densification phenomenon of the films is the result of the high bombardment energy of the growing films, which increase according to the bias growth. Wang et al. reported that the CrNbTiMoZr film deposited without bias voltage exhibited an island-like surface structure [64]. All films were deposited at different substrate biases, and the surface morphology became denser and smoother with increasing bias. Regarding the cross-section of films, the results revealed changes from a columnar structure to a fine fiber structure by increasing the bias. The study of a $(Al_{1.5}CrNb_{0.5}Si_{0.5}Ti)_{50}N_{50}$ film reveals a surface with a cauliflower-like morphology obtained at 0 V (Figure 4a) that changes to a smooth morphology, as shown in Figure 4b, and a featureless surface is obtained at −150 V (Figure 4c) [29]. More analysis, presented in the same reference, reported that the SEM cross-sectional micrographs (not presented here) display a morphology change: a columnar shape is formed at 0 V, it becomes dense at −50 V, while at −150 V a featureless appearance is observed.

Other studies revealed the dependence of HEF morphology on the substrate temperature. When the temperature increases, the morphology becomes dense. Islands were observed in the case of FeCoCrNiMoO HEF, as shown in the Figure 4 [65]. By increasing the substrate temperature, the size of the islands was decreased leading to a dense morphology. This is due to the increase in the energy of the surface adatoms when the temperature became higher. Smooth grains were formed at room temperature in the form of sheets. A FeCoNiAlMnW film deposited at 200 °C showed two types of grains, polyhedral with a size of 100−150 nm and other tiny grains with a size of 20−30 nm [66]. As the temperature increases, the ultrafine grains became larger with a size ranging between 60 and 100 nm.

Behravan et al. [67] reported the preparation of AlSiTiCrMo oxide using unbalanced DCMS under a pressure effect, which was altered between 1 and 8 mTorr. The film obtained at 1 mTorr shows a morphology devoid of defect-free features. The one deposited at 4 mTorr shows a surface with some nodular grains. This morphology is related to the low energy of the atoms on the surface caused by an increase in the pressure. At 8 mTorr, the surface size of nodular grains increases.

An $AlCoCrCu_{0.5}FeNi$ film deposited at different oxygen flow fractions showed a surface with grains of various sizes [26]. At low oxygen flow, the film surface showed agglomerated grains with an average cluster size of 88 ± 2 nm. When O_2 flow increased, the grains became equiaxed with a size of 35 ± 1 nm. Chen et al. reported the change of the surface morphology of VAlTiCrMo film after the introduction of the nitrogen [24]. The metallic composition presented a surface of a regular tetrahedral particles. The size of the particles increased when the nitrogen content increased, leading to a smooth and compact surface.

An (AlCrNbYZr) film has been studied by changing the nitrogen flow rate. The metallic film showed a dendrite-like microstructure, as shown in Figure 4d [25]. However, as the nitrogen increased, the morphology changed. A V-shaped columnar morphology was formed at 46 at.% N with trigonally shaped grains formed on the surface of the film (Figure 4e). At 51 at.% N, the morphology became smoother with small, rounded grains

(Figure 4f). On the other hand, nanoparticles with different geometries as a function of nitrogen content were reported for the film FeCoNiCuVZrAl [68]. Without nitrogen, the nanoparticles had a size of about 10−25 nm, and the surface became smooth by increasing the nitrogen content.

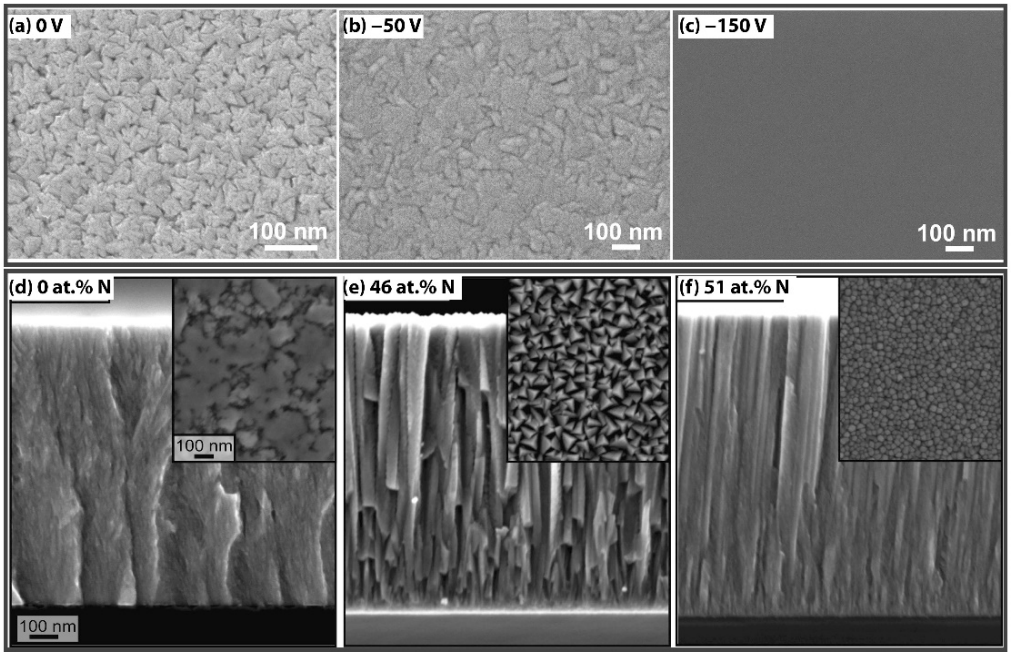

Figure 4. $(Al_{1.5}CrNb_{0.5}Si_{0.5}Ti)_{50}N_{50}$ film at 0 V (**a**), −50 V (**b**) and −150 V (**c**). (AlCrNbYZr)N films with different N content at 0 at.% (**d**), 46 at.% (**e**) and 51 at.% (**f**). Figures are reproduced and modified with permission of ref. [29] for (**a**–**c**) copyright 2012 Thin Solid Films and of [25] for (**d**–**f**). Copyright 2020 Surf. Coat. Technol.

4.1.2. Structure

The reported HEFs, deposited by magnetron sputtering, are crystalline or amorphous. Under the substrate bias effect, some HEFs showed crystalline phase [29,30,64], while other films were not influenced [63]. For example, the (AlCrSiNbZr)N HEF exhibited a NaCl-fcc phase with substrate biases of 0 V, −25 V, −50 V and −75 V [30]. However, in the case of the CrNbSiTiZr film, no effect on its crystal structure was observed [63]. Behraven et al. summarized some HEFs prepared with different deposition parameters, revealing the formation of an amorphous structure [67]. According to various reports, substrate temperature, substrate bias and working pressure have no effect on the phase of different HEFs, except in the study reported by Khan et al., where a phase transformation of $AlCoCrCu_{0.5}FeNi$ from disordered to crystalline structure occurred by changing the pressure.

Table 1 summarizes the different crystalline structures of HEFs prepared by magnetron sputtering in the last 10 years. The most reported films exhibit an fcc solid solution structure. This reveals the influence of the gases on the phase transformation of the films. In the case of HECF, Jhon et al. reported the formation of an fcc structure of CrNbSiTiZr resulting from NbC, TiC and ZrC forming binary carbides [21]. As the carbon content increased, the films became amorphous. The same behavior was observed in the case of some HEOF. A bcc solid solution phase was formed of (NbMoTaWV)O film at 16 at.% of O_2. However, when the O content increased, the film became amorphous. In addition, $AlCoCrCu_{0.5}FeNi$ and $FeCrCoNiAl_{0.1}$ HEO revealed the formation of an fcc solid solution structure at a low at.% of O with a spinel structure at high content of O [26,69].

Table 1. Reported crystalline structure of HECF, HEOF and HENF prepared by magnetron sputtering in the last 10 years.

Composition	Gas	Structure		[Refs.]
		Without Gas	With Gas	
CrNbSiTiZr	CH_4	unmentioned	fcc	[21]
$FeCrCoNiAl_{0.1}$	O_2	fcc	fcc (spinel)	[69]
$AlCoCrCu_{0.5}FeNi$	O_2	unmentioned	fcc (spinel)	[26]
NbMoTaWV	O_2	bcc	amorphous	[70]
$Al_{0.19}Cr_{0.13}Nb_{0.19}Ta_{0.30}Ti_{0.19}$	O_2	unmentioned	rutile-type (r-TiO_2)	[19]
AlCrTiVZr	N_2	amorphous	fcc	[57]
NbTaMoW	N_2	bcc	fcc	[71]
MoNbTaVW	N_2	bcc	fcc	[72]
CrNbTiAlV	N_2	amorphous	fcc	[73]
$Cr_{0.35}Al_{0.25}Nb_{0.12}Si_{0.08}V_{0.20}$	N_2	amorphous	B1-NaCl	[74]
MoNbTaVW	N_2	bcc	fcc	[13]
AlTiTaZrHf	N_2	amorphous	fcc	[75]
VAlTiCrMo	N_2	bcc	fcc	[24]
AlCrTiZrV	N_2	amorphous	fcc	[76]
AlCrNbYZr	N_2	nanocomposite	fcc	[77]
$AlCoCrCu_{0.5}FeN$	N_2	unmentioned	fcc + fcc	[78]
AlCrTiZrHf	N_2	amorphous	fcc	[59]
NbTiAlSiZr	N_2	amorphous	amorphous	[79]
AlCoCrNi	N_2	amorphous	amorphous	[27]
$Al_{0.5}CrFeNiTi_{0.25}$	N_2	amorphous	fcc	[80]
FeCoNiCuVZrAl	N_2	amorphous	amorphous	[68]
ZrTaNbTiW	N_2	amorphous	bcc + fcc	[81]
AlCrMoNiTi	N_2	amorphous	bcc	[82]
AlCrMoZrTi	N_2	amorphous	bcc	[82]
TiZrNbHfTa	N_2	fcc + intermetallic	fcc	[83]
AlCrMoTaTiZr	N_2	amorphous	fcc	[20]

In the case of HENF investigations, without nitrogen, most reported films deposited by magnetron sputtering are amorphous. An example is shown with XRD diffractograms from reference [20], which are presented in Figure 5a. Figure 5b shows a large peak, as reported in reference [76], indicating the amorphization of the film without the nitrogen. However, an fcc solid solution was obtained upon increasing the nitrogen content, as presented in Figure 5a,b. The adsorption of the nitrogen atom in interstitial sites promoted the phase transformation of the film, resulting in the crystalline structure. Some analyses reported that HENF exhibit fcc phased solid solution due the formation of binary nitrides having the same structure. However, this rule cannot be generalized. Some HEFs remain amorphous, even after increasing the nitrogen content, such as in the case of NbTiAlSiZr [79], AlCoCrNi [27], FeCoNiCuVZrAl [68] and AlBCrSiTi [84] nitrides films. Liu et al. explain that the amorphization tendency could result from the low enthalpy of the mixed elements, the difference between the depositing temperatures and also from a large solid/liquid interface energy [68]. On the other hand, other HENFs present a mixed bcc and fcc structure after increasing the nitrogen content, as in the case of ($AlCoCrCu_{0.5}FeNi$)N [78] and (ZrTaNbTiW)N [81]. The authors explain that the formation of these mixed phases is caused by

increasing the nitrogen because only some part of the alloys form nitrides. Other element, such as Nb and W, are bcc and promote the formation of a bcc phase.

The change in the crystalline structure of these HEFs could be a result of a competition between many parameters. Even though high entropy prevents the formation of intermetallic compounds and promotes the formation of solid solutions, the difference in the atomic size leads to lattice distortion. If this latter is high enough, HEFs remain amorphous, even after adding the gas. However, when the metallic elements have close atomic radii, a crystalline structure can be formed after the introduction of the gas. In general, three different phased structures, amorphous, fcc and bcc, are reported in the case of HEF investigations. While the changes from amorphous to crystalline structure may be due to the mutual solubility and similar structure of nitrides, more investigations are needed to provide an in-depth explanation of the amorphization formation tendency after adding the reactive gas.

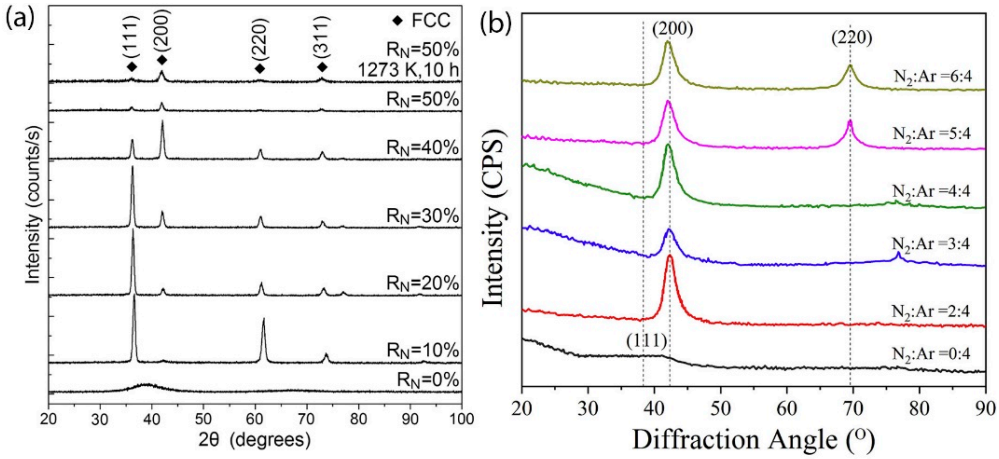

Figure 5. X-ray diffractograms showing the evolution of the structure as a function of the nitrogen flow rate. (**a**) reproduced and modified with permission ref. [20] copyright 2011 Thin Solid Films. (**b**) reproduced and modified with permission of ref. [76]. Copyright 2020 Vacuum.

4.2. Mechanical and Tribological Properties

4.2.1. Hardness

The mechanical properties of HEFs are strongly dependent on their microstructure. A dense microstructure of film can result from the high mobility of sputtered atoms presenting high hardness. Lin et al. reported the reduction of residual stress and the annihilation of vacancies in $(Cr_{0.35}Al_{0.25}Nb_{0.12}Si_{0.08}V_{0.20})N$ film by increasing the temperature, resulting in improved hardness [28]. In the case of FeCoNiAlMnW film, Sun et al. [66] observed a fluctuated variation of the hardness by changing the temperature of the substrate.

The hardness and Young's modulus could also be influenced by the substrate bias parameter. A CrNbSiTiZr film obtained at -50 V showed high compressive residual stress of -0.82 ± 0.04 GPa [63]. The hardness increased significantly and reached a maximum of 12.4 ± 0.3 GPa at -50 V bias, and then decreased to 9.8 ± 0.2 GPa at -200 V bias. Young's modulus increased with the increase in the substrate bias to 187.7 ± 3.3 GPa at -100 V, followed by a decrease to 162.3 ± 3.7 GPa when the bias was -200 V.

Furthermore, the highest mechanical properties of the films were obtained at the pressure of 1.33×10^{-1} Pa, with a hardness of 16.8 ± 0.5 GPa and a modulus of 243 ± 39 GPa, respectively. Khan et al. [85] reported no change in the mechanical properties in the case of $AlCoCrCu_{0.5}FeNi$ film as a function of working pressure. The mechanical properties were measured at 13 GPa for hardness and more than 204 GPa for Young's modulus.

For HEOF, the hardness and Young's modulus of $(Al_{0.19}Cr_{0.13}Nb_{0.19}Ta_{0.30}Ti_{0.19})O_2$ increased slightly from 22 to 24 GPa, and from 380 to 400 GPa, respectively. The study revealed a change in the hardness, and the maximum value was measured at 11 GPa

with 25% oxygen flow. HECF also experienced a strong change in hardness and Young's modulus (Table 2). As the carbon content increases, the mechanical properties of HEFs decreases, and this was observed for (CrNbSiTaZr)C films. Table 2 summarizes hardness, Young's modulus and the friction coefficient of different HEFs prepared by magnetron sputtering. Compared to HECF and HEOF, HENF demonstrates the increase in their mechanical properties as the nitrogen content increases (Table 2). For example, the hardest HENF was obtained for (AlCrMoTaTiZr)N with a 40% nitrogen flow ratio. Its hardness was measured at 40 GPa and the Young's modulus ranged from 370 to 420 GPa, depending on the nitrogen flow.

Table 2. Hardness, Young's modulus (only high values) and friction coefficient (low values) of HEFs prepared by magnetron sputtering, at different parameters, in the last 10 years. The values highlight the best obtained results of each study.

Composition	Hardness (GPa)	Young Modulus (GPa)	Friction Coefficient (Counterpart)	[Refs.]
FeCoNiAlMnW	8.08	187–200	-	[66]
(AlCrNbSiTiV)N	2493 HV	-	0.78 (Al_2O_3 ball)	[61]
(AlCrMnMoNiZr)N	15.2	221	0.12 (Si_3N_4 ball)	[82]
(TiVCrZrHf)N	48	316	-	[22]
CrNbSiTiZr	12.5	187.7	0.53 (GCr15 ball)	[63]
CrNbTiMoZr	9.7	150.1	~0.5 (GCr15 ball)	[64]
(AlCrSiNbZr)N	9.8	-	-	[30]
AlCrFeCoNiCuV	9	225	-	[86]
AlCrTiWNbTa	12.5	181	-	[64]
(Al1.5CrNb0.5Si0.5Ti)N	36	350	-	[29]
AlCrSiTiMoO	8.9	196	-	[67]
(CrNbSiTaZr)C	20.12	-	0.05 (Si_3N_4 ball)	[87]
(CrNbSiTaZr)C	32.8	358	0.07 (100Cr6 ball)	[21]
(TiZrNbHfTa)C	27.5	-	0.15 (sapphire ball)	[83]
(AlCoCr$Cu_{0.5}$FeNi)O	8.2	140	-	[26]
(NbMoTaWV)O	15.4	212.12	-	[70]
(AlCrNbTaTi)N	24	400	-	[19]
(MoNbTaVW)N	30	-	-	[72]
(VAlTiCrMo)N	5.55	152.01	-	[24]
(AlCrTiZrV)N	34	328	-	[76]
(AlCrNbYZr)N	29.6	343	-	[25]
(AlCrTiZrHf)N	33.1	347.3	0.5 (GCr15 ball)	[59]
(NbTiAlSiZr)N	29.6	184.5	-	[79]
($Al_{0.5}$CrFeNi$Ti_{0.25}$)N	21.78	253.8	-	[80]
(FeCoNiCuVZrAl)N	~11.5	~165	-	[68]
(ZrTaNbTiW)N	~17	~144	-	[81]
(AlCrMoNiTi)N	19.6	236	~0.22 (Si_3N_4 ball)	[60]
(AlCrMoZrTi)N	15	263	~0.14 (Si_3N_4 ball)	[60]
(TiZrNbHfTa)N	32.29	-	0.87 (sapphire ball)	[83]
(AlCrMoTaTiZr)N	40.2	400	0.74 (100Cr6 ball)	[20]

4.2.2. Tribological Properties

The evolution of the mechanical and tribological properties of HEFs, mentioned above, seem to be influenced by different parameters, such as the substrate temperature, bias voltage, alloy element, pressure and reactive gases. The microstructure evolution could be a result of a change in the preferred orientation, crystallite size and densification phenomenon of the films. All these phenomena improve the mechanical and tribological performance of the films. Other studies demonstrate that residual stresses also have a significant effect on hardness [88]. These studies explain that the residual stresses result from the incorporation of defects that will prevent the plastic flow during deformation, resulting then in a change in hardness.

Kuang et al. [89] reported the reduction of the friction coefficient of CrNbTiMoZr carbides. The films were prepared by changing the bias voltage. The incorporation of carbon may produce a lubricating effect, reducing the friction coefficient. The wear resistance was showed to decrease as the bias voltage increased. Cui et al. [90] studied the effect of Al on the performance of $FeCoCrNiMnAl_x$. The results showed a decrease in the friction coefficient as Al content increased. Regarding the wear of the film, the results revealed that the cladding layers changed from adhesive to abrasive wear as the Al content increased. On the other hand, Wang et al. [64] revealed no effect of the bias voltage on the friction coefficient of CrNbTiMoZr films. They estimated the tribological performances of the films from their mechanical properties. The influence of the bias voltage on the wear resistance of the films was linked to the deformation mechanism. Lo et al. [91] studied the tribological performance of (AlCrNbSiTiMo)N at room temperature (RT) and after heating at 700 °C. They showed a reduced friction coefficient of the film at 700 °C (0.48 ± 0.08) compared to that at RT (0.68 ± 0.09). This is due to the formation of MoO_3 after annealing, which acts as lubricating effect. The wear resistance was then improved.

Wear resistance can be predicted using the elasticity index (H/E) and the plasticity index (H^3/E^2). Jhong et al. [21] show the high E/H and H^2/E^3 values $(CrNbSiTiZr)C_x$ of compared to that of conventional alloys. The carbide with 87.8 at. % of carbon showed better wear resistance. Recently, Kao et al. [87] used acetylene (C_2H_2) with a flow ranging from 0 to 23 sccm to prepare CrNbSiTaZr HEF through RF magnetron sputtering. The metal composition, i.e., without C_2H_2 had high hardness (20.12 GPa) but low tribological properties. By increasing the C_2H_2 flow, the hardness of carbides decreased. The maximum value obtained for the carbides was about 14 GPa, and this was for the film obtained with the 9 sccm C_2H_2 flow. This film has the lowest wear rate. Heat treatments of the film were performed at 750 °C, resulting in a change in the mechanical and tribological properties. The hardness and critical load of the coatings decreased following a transformation from a predominant DLC structure to a graphite structure.

4.3. Corrosion Behaviour

4.3.1. Corrosion in Liquid

Corrosion significantly affects many materials. A degradation of the alloys occurs and leads to economic losses. The development of corrosion-resistant materials can help to resolve the problem and increase their performance. Developing HEFs as coatings with good corrosion resistance is of great interest and should be pursued in many applications. HEFs are advantageous due to the formation of solid solutions rather than intermetallic compounds. Several HEFs have been fabricated by magnetron sputtering and shown to have better corrosion resistance. This has been studied and discussed under the effect of various parameters. Below, some parameters affecting the corrosion behavior of HEFs are presented and discussed.

4.3.2. Effect of Composition

The elemental content has been reported to influence the electrochemical properties of HEFs. Bachani et al. [92] improved the corrosion resistance of a 304 stainless steel substrate in 0.5 M H_2SO_4 solution. This was achieved by adding Al in the refractory VNbMoTaW

HEF films. The results revealed that the film with 2.37 at.% Al has excellent corrosion resistance compared to 304 stainless steels. However, increasing the percentage of Al tends to form a porous oxide which can be easily affected by the acid. As the Al content increases, the oxide film becomes more porous and, consequently, the corrosion resistance decreases. The same material, VNbMoTaW, was also investigated in 3.5% aqueous NaCl solution, with the addition of a significant amount of two elements, Cr and B [93]. Since the corrosion resistance is strongly linked to the microstructure, the film without B is columnar, and this microstructure can be easily attacked by the salt. However, increasing the B content makes the microstructures denser and improves the corrosion resistance of the films. Varying the content of some other component of HEFs also confirms this trend. In fact, when increasing the content of Fe-Co-Ni, Wang et al. reported and improved the corrosion resistance of (Fe-Co-Ni)$_x$(Al-Ti-Zr)$_{100-x}$ [94]. Among the different films, (Fe-Co-Ni)$_{25}$(Al-Ti-Zr)$_{75}$ showed better anti-corrosion performance. The morphology changed according to the elemental contents, which strongly affected the corrosion behavior of the materials. Malinovskis et al. studied the anti-corrosion performance of (CrNbTaTiW)C in 1 M HCl [23]. The properties of these films were compared with those of hyper-duplex stainless steel. The results revealed that all the carbides showed good corrosion resistance. Among the different carbides, the best resistance was observed for the Ta/W-rich film, confirming that elemental content has an effect on HEFs' performance.

4.3.3. Effect of Substrate Bias and Temperature

Other parameters, such as substrate bias and temperature, strongly influence the anti-corrosion performance of the films. Von Fieandt et al. [77] studied (AlCrNbYZr)N$_x$ in HCl by changing the bias voltage and temperature parameters. They showed an improved corrosion resistance of the films compared to both hyper-duplex stainless steel and compared to (Nb,Zr)N$_{0.90}$ thin film. High corrosion resistance was found for the film obtained at −150 V and at temperature of 700 °C. With these conditions, the film had a low surface roughness and high density. Kao et al. reported that the corrosion resistance of the films prepared with C_2H_2 flux was significantly improved after a heat treatment. Under the temperature effect, an oxide layer was formed on the film surface, which prevented the corrosion affect [87]. The good resistance was due to the high density and low roughness of the films. The properties of these HEFs were compared with those of the WC substrates. The results revealed that the annealing process of HEFs improves their anti-corrosion performance.

4.3.4. Oxidation at High Temperature

Feng et al. [95] investigated the temperature oxidation of multi-element TaNbTiW film. The film shows thermal stability at up to 900 °C. However, by increasing the temperature, oxides such as Ta_2O_5, NbO_2 and Nb_2O_5 are formed. Using a pressure of 10^{-3} Pa, oxygen residue leads to film oxidation under the annealing effect. The authors reported that films with high W content had a good resistance to oxidation. Moreover, increasing both Ti and W content led to the densification of the film, preventing the diffusion of oxygen. Shen et al. [16] reported the superior oxidation resistance of $(Al_{0.34}Cr_{0.22}Nb_{0.11}Si_{0.11}Ti_{0.22})_{50}N_{50}$. The film annealed at 900 °C for 50 h presented two oxides: α-Al_2O_3 and rutile-TiO_2. By increasing the temperature to 950 °C for 10 h, the quantity of the oxides increased. At 1000 °C, Cr_2O_3 was also formed. The performance of the films was compared to those of TiN and TiAlN under the same conditions, and $(Al_{0.34}Cr_{0.22}Nb_{0.11}Si_{0.11}Ti_{0.22})_{50}N_{50}$ had a remarkable oxidation resistance. The formation Al_2O_3 as a top layer with a dense microstructure is the main reason for improving the oxidation resistance. $(Al_{23.1}Cr_{30.8}Nb_{7.7}Si_{7.7}Ti_{30.7})_{50}N_{50}$ and $(Al_{29.1}Cr_{30.8}Nb_{11.2}Si_{7.7}Ti_{21.2})_{50}N_{50}$ films were isothermally annealed at 900 °C for 2 h in air [88]. Both films showed good oxidation resistance. SEM characterization reveals that numerous oxide particles formed on the surface of both films. The thickness of the oxides was estimated on the cross-sectional SEM images to be around 100 ± 12 nm for $(Al_{23.1}Cr_{30.8}Nb_{7.7}Si_{7.7}Ti_{30.7})_{50}N_{50}$ and 80 ± 7 nm

for $(Al_{29.1}Cr_{30.8}Nb_{11.2}Si_{7.7}Ti_{21.2})_{50}N_{50}$. The films had a high oxidation resistance compared to that of many conventional coatings, such as CrN annealed at 800 °C for 2 h. Moreover, $(Al_{29.1}Cr_{30.8}Nb_{11.2}Si_{7.7}Ti_{21.2})_{50}N_{50}$ presents better oxidation resistance compared to $(Al_{23.1}Cr_{30.8}Nb_{7.7}Si_{7.7}Ti_{30.7})_{50}N_{50}$. The content of some elements can strongly influence the oxidation properties of films. It is known that Al_2O_3 is generally dense and prevents the diffusion of oxygen into the film, while Rutile-TiO_2 is less protective. The dense microstructure eliminates oxygen transport channels and increases the anti-oxidation resistance of the films. (AlCrMoTaTi)N was investigated between 733 K and 1073 K [96]. The results revealed that the addition of Si in the films significantly improved their oxidation resistance. The good anti-oxidation performance of the films can be due to the protective α-Al_2O_3 and α-SiO_2 layers. Kretschmer et al. [17] studied also the oxidation behavior of (AlCrNbTaTi)N film in air as a function of Si concentration. The annealing was performed at 850°C for 100 h. Without Si, the film showed an oxide thickness of 2700 nm, while those with Si had 280 nm (Figure 6). The addition of Si in the films led to the formation of a dense microstructure that slowed down the diffusion of oxygen.

The oxidation of HEFs under ambient conditions was also reported. Hruska et al. used XPS to study the oxidation of HfNbTaTiZr film in ambient air [97]. Oxygen absorbed from the atmosphere reacted with Ti, Zr, Nb, Hf and Ta atoms, forming oxide nanoclusters. The study points out that only XPS revealed an oxygen content of 66 at.% compared to other techniques, namely, SEM, TEM and X-ray diffraction analysis, where no oxide was determined. A depth profiling of the films with argon ions was carried out to analyze the oxidation behavior and estimate the O content. The depth increased as the O content decreased. The O was found to be preferentially bound to Ti, Zr and Hf rather than Nb and Ta. The oxygen diffusion in the film may be due to the porous structure.

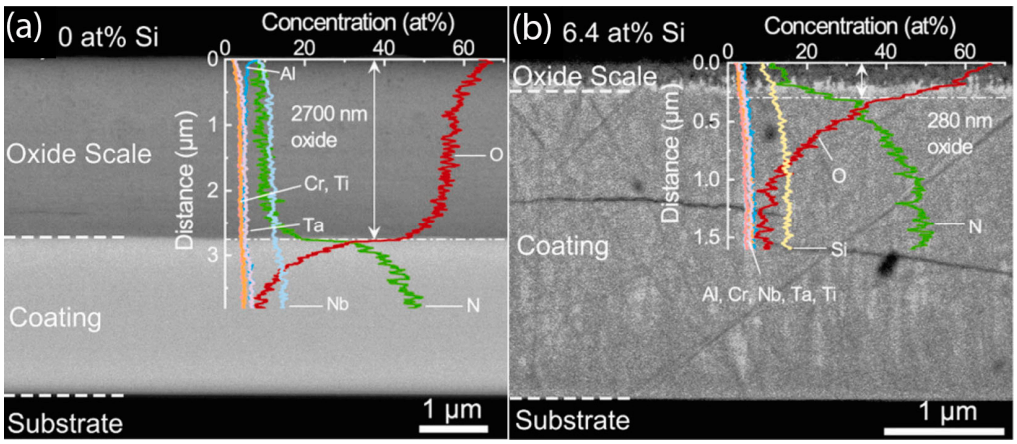

Figure 6. SEM cross-section of the (AlCrNbTaTi)N without Si (**a**) and with 6.4 at.% Si (**b**) after exposure to ambient air at 850 °C for 100 h. Figure reproduced with permission ref. [17]. Copyright 2021 Surface and Coatings Technology (open access).

4.4. Thermal Stability

This subsection focusses on the recent results of the studies of the thermal stability of HEFs. Their microstructural and mechanical properties remain stable even at high temperatures. Kirnbauer et al. [98] reported on the thermal stability and mechanical properties of $(HfTaVWZr)B_2$ film when changing the substrate bias. A single phase AlB_2 structure was formed that remained unchanged even after vacuum annealing at 1300 °C. However, by increasing the temperature to 1400 °C, an additional (V,W)B phase was formed with $(Hf,Ta,Zr)B_2$ as a matrix (Figure 7). The mechanical properties of the annealed film decreased as the temperature increased. The same group has also studied HfTaTiVZr nitrides [50]. No significant change in the structure (fcc) was observed after annealing at 1300 °C, revealing their stability at this temperature. However, when annealing the films at temperatures above 1400 °C, a hexagonal $(Ta,N)_2N$ phase was formed. Nitrogen

desorption can be the main reason for the phase transformation. Cemin et al. [99] point out that the formation of phases can be due to the thermodynamic and kinetic growth process. AlSiTaTiZr was thermally studied at between 673 and 836 K. The results showed that the films were stable at 823 K, but upon increasing the temperature (848 K), several intermetallic compounds were formed. Theoretical calculations using CALPHAD were carried out to obtain an in-depth understanding of the thermal behavior of these films. The results revealed that the formation of intermetallic compounds was prompted by the large content of Al and Si due to the exceedance of the enthalpy contribution compared to the entropy.

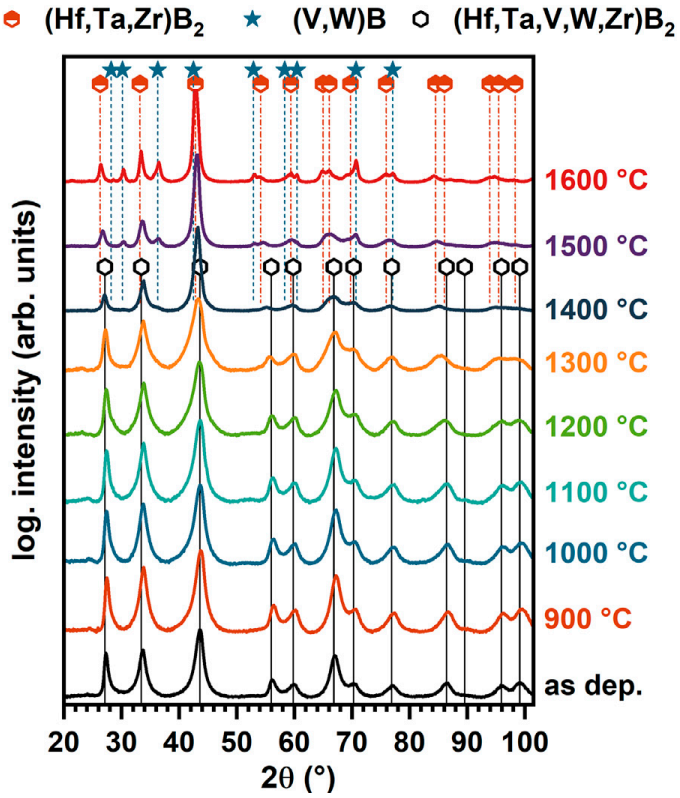

Figure 7. X-ray diffraction patterns of vacuum-annealed (HfTaVWZr)B_2 at different temperatures. Figure reproduced with permission ref. [98]. Copyright 2020 Acta Materialia.

5. Applications

Various reported works on HEFs deposited by magnetron sputtering have been performed to enhance their properties compared to the conventional coatings. The new materials can serve in different applications as their surfaces have superior performances. This section includes the property requirements for some applications of magnetron-sputtered HEFs.

5.1. Biomedical Application

Three groups of materials are now being considered for use as biomedicals, namely, SS304, Ti and CoCr alloys. Considerable scientific research has been focused on protective coatings that improve the performance of implants and prostheses. In the case of HEFs, Braic et al. [100] studied the potential carbides and nitrides for biomedical applications. Two films, (HfNbTaTiZr)N and (HfNbTaTiZr)C, have been prepared by magnetron sputtering and the corrosion property was simulated in body fluid. Biocompatibility tests have shown that the coatings did not induce any cytotoxic response after 24 h and 72 h. A good morphology of the attached cell was observed. The cell analysis revealed a very high ratio between the live and the dead cells. A very small ratio of dead cells was

observed for (HfNbTaTiZr)N and (HfNbTaTiZr)C coatings. Valdescu et al. [101] also studied the biocompatibility of (TiZrNbTaHf)C by replacing some elements (Ti or Ta) with Si. They found that this replacement led to improved biocompatible properties, where a (TiZrNbSiHf)C coating showed the best biocompatibility. Codescu et al. [102] functionalized FeMoTaTiZr using hydroxyapatite-based coatings to increase their biocompatibility and corrosion resistance so that they could be used as bone implants. The alloy was prepared by vacuum arc remelting, but the coating was obtained using the RF magnetron sputtering method. The final material has been prepared to serve as a biodegradable material for medical application.

5.2. Diffusion Barrier Application

Copper is used as a preferred interconnecting material, but its adhesive ability with a dielectric layer is low. Copper can easily diffuse in silicon as the temperature increases. A barrier material is needed to improve the reliability and the stability of such material. Peng et al. [103] studied a TiVCrZrHf HEF deposited by magnetron sputtering on Si/SiO_2 as a barrier layer for copper. The results revealed that HEF retarded the diffusion of copper at temperatures below 600 °C. A failure was observed at 700 °C, since TiVCrZrHf crystallized and an interdiffusion between the coating and copper occurred. Due to its structural and thermal stability being below 600 °C, HEF can be a candidate barrier material for copper interconnections. In addition, Li et al. [104] examined AlCrTiTaZrMo nitride as a barrier layer for copper metallization. They characterized its thermal stability and barrier performance between 400 °C and 900 °C. A nanocomposite structure without grain boundaries with a large lattice distortion were the main factors leading to barrier layer behavior. $(AlCrTiTaZrMo)N_{0.2}$ was found to have excellent barrier resistance and was the best candidate for barrier material.

5.3. Wear Resistance Application

Wear is one of the known problems that affects various materials used in different industry fields. The used material should have high mechanical performance to meet industrial needs. The tribological performances of $(CrAlTiNbV)N_x$ have been tested in 4050 aviation lubricant, revealing a low value for the friction coefficient (0.096) and wear rate (1.8×10^{-7} $mm^3/(N{\cdot}m)$) [105]. The best performance of $(CrAlTiNbV)N_x$ was due to its characteristics, namely, it was the densest and had a fine columnar structure and good mechanical properties. HEF nitrides again confirm their potential to outperform the other materials used in various metallurgical fields.

5.4. Machining Application

In the last decade, the dry machining process has been of a great interest as a replacement for fluid in industry. Coatings are being developed to prolong the lifespan of tools and improve their performances. Shen et al. [106] have investigated an $(Al_{0.34}Cr_{0.22}Nb_{0.11}Si_{0.11}Ti_{0.22})_{50}N_{50}$ HEF, prepared by reactive magnetron sputtering, and have examined its thermal and machining properties. They reported that the cutting performances of the coating were better as the milling is operated at high temperature. Compared to other basic nitrides, this HEF is advantageous due to its combined high hardness, good thermal stability and outstanding oxidation resistance. With continuous machining at high speed (160 m/min), the wear depth of the $(Al_{0.34}Cr_{0.22}Nb_{0.11}Si_{0.11}Ti_{0.22})_{50}N_{50}$ HEF coated insert was 23% and 25% smaller than that of TiN and TiAlN, respectively. This demonstrates that HEFs can outperform their commercial counterparts in industry.

6. Conclusions and Outlooks

HEFs have become the focus of many investigations and analyses. It has been shown that the films exhibit attractive and unique properties compared to conventional alloys. In general, HEFs exhibit have high oxidation temperatures, good tribological performances and better corrosion resistance compared to standard PVD films. This paper focused on

HEFs prepared using the magnetron sputtering technique and their properties. Changing the parameters strongly influences the chemical, the physical and mechanical properties, leading to films with high performances. The main contents of the paper can be summarized as:

- The working principle of magnetron sputtering and the process of HEF preparation has been presented. Standard sputtering (direct current) and high-power impulse magnetron sputtering (HiPIMS) were discussed.
- The effect of different magnetron sputtering parameters on the physico-chemical properties of HEFs was analyzed and discussed. The substrate bias voltage, the substrate temperatures and the flow of the gases (N_2, O_2 and CH_4/C_2H_2) strongly influence various properties of HEFs. Single phases and intermetallic compounds are formed. The deposition rates decrease as the magnetron parameters are changed.
- The mechanical properties of HEFs have been summarized, and they show that the films exhibit high hardness, Youngs modulus and wear resistance. Nitride films have been reported to be super hard due to the high density of their microstructure. The latter can be controlled by controlling the magnetron sputtering parameters.
- The paper focuses mainly on the analysis of two properties of HEFs, namely, electrochemical and physical (thermal) properties. Corrosion has been reported to be influenced by several parameters: the content/type of the elements constituting the HEFs, the polarization voltage and the substrate temperature. It has been shown that the formation of dense films with low surface roughness prevents the penetration of the corrosive solution.
- HEFs prepared by magnetron sputtering show better oxidation resistance at high temperature compared to conventional films. Oxides, such as Al_2O_3, that form on the surface of the films act as barriers to oxygen diffusion and protect the films.
- HEFs also showed good thermal stability at high temperatures. The value of the threshold temperature depends on each composition, but in general, HEFs are thermally more stable compared to the conventional films. Ceramic HEFs, especially nitrides, are stable at temperatures reaching 1000 °C. However, at temperatures above 1000 °C, intermetallic compounds are formed. The large difference between the enthalpy and entropy is the main reason for the phase transformation.
- Due to their high performances, HEFs prepared by magnetron sputtering demonstrated their potential as protective coatings that can be used for various applications, such as in biomedicine, barrier diffusion, wear resistance and machining tools.

Intensive studies are still being performed for the preparation, the development and the control of HEFs' properties. Attractive properties of the films have been ascertained by controlling the different parameters of the magnetron sputtering process. However, some points still need to be deeply investigated. First, the relationship between the configurational entropy and the properties of HEFs merits further study. In the case of nitrides, the mechanism of the phase transformation from an amorphous to crystalline structure after the addition of nitrogen needs to be elucidated. The effect of nitride-forming and non-nitride-forming elements must be studied. An important point concerns the selection criteria that give different results between bulk materials and thin films. Calculations and theoretical studies need to be explored in this field.

Author Contributions: M.E.G.: Conceptualization, writing—original draft preparation, review and editing, P.B.: review and editing, F.S.: writing, review and editing. All authors have read and agreed to the published version of the manuscript.

Funding: This research received no external funding.

Acknowledgments: The authors thank the Université de Technologie de Troyes (UTT) and le Conseil départemental de l'Aube (CD10).

Conflicts of Interest: The authors declare no conflict of interest.

References

1. Miracle, D.B.; Senkov, O.N. A critical review of high entropy alloys and related concepts. *Acta Mater.* **2017**, *122*, 448–511. [CrossRef]
2. Senkov, O.N.; Miller, J.D.; Miracle, D.B.; Woodward, C. Accelerated exploration of multi-principal element alloys with solid solution phases. *Nat. Commun.* **2015**, *6*, 6529. [CrossRef]
3. Cantor, B.; Chang, I.; Knight, P.; Vincent, A. Microstructural development in equiatomic multicomponent alloys. *Mater. Sci. Eng. A* **2004**, *375*, 213–218. [CrossRef]
4. Gao, M.C.; Yeh, J.-W.; Liaw, P.K.; Zhang, Y. *High-Entropy Alloys*; Springer: Cham, Switzerland, 2016.
5. Yeh, J.-W. Recent progress in high entropy alloys. *Ann. Chim. Sci. Mater.* **2006**, *31*, 633–648. [CrossRef]
6. Chuang, M.-H.; Tsai, M.-H.; Wang, W.-R.; Lin, S.-J.; Yeh, J.-W. Microstructure and wear behavior of $AlxCo_{1.5}CrFeNi_{1.5}Tiy$ high-entropy alloys. *Acta Mater.* **2011**, *59*, 6308–6317. [CrossRef]
7. Wu, Y.D.; Cai, Y.H.; Wang, T.; Si, J.J.; Zhu, J.; Wang, Y.D.; Hui, X.D. A refractory $Hf_{25}Nb_{25}Ti_{25}Zr_{25}$ high-entropy alloy with excellent structural stability and tensile properties. *Mater. Lett.* **2014**, *130*, 277–280. [CrossRef]
8. Chen, Y.Y.; Duval, T.; Hung, U.D.; Yeh, J.W.; Shih, H.C. Microstructure and electrochemical properties of high entropy alloys—A comparison with type-304 stainless steel. *Corros. Sci.* **2005**, *47*, 2257–2279. [CrossRef]
9. Chen, Y.Y.; Hong, U.T.; Shih, H.C.; Yeh, J.W.; Duval, T. Electrochemical kinetics of the high entropy alloys in aqueous environments—A comparison with type 304 stainless steel. *Corros. Sci.* **2005**, *47*, 2679–2699. [CrossRef]
10. Ma, S.G.; Zhang, S.F.; Gao, M.C.; Liaw, P.K.; Zhang, Y. A successful synthesis of the $CoCrFeNiAl_{0.3}$ single-crystal, high-entropy alloy by Bridgman solidification. *JOM* **2013**, *65*, 1751–1758. [CrossRef]
11. Glasscott, M.W.; Pendergast, A.D.; Goines, S.; Bishop, A.R.; Hoang, A.T.; Renault, C.; Dick, J.E. Electrosynthesis of high-entropy metallic glass nanoparticles for designer, multi-functional electrocatalysis. *Nat. Commun.* **2019**, *10*, 2650. [CrossRef] [PubMed]
12. Schuh, B.; Völker, B.; Todt, J.; Schell, N.; Perrière, L.; Li, J.; Couzinié, J.P.; Hohenwarter, A. Thermodynamic instability of a nanocrystalline, single-phase TiZrNbHfTa alloy and its impact on the mechanical properties. *Acta Mater.* **2018**, *142*, 201–212. [CrossRef]
13. Xia, S.; Gao, M.C.; Yang, T.; Liaw, P.K.; Zhang, Y. Phase stability and microstructures of high entropy alloys ion irradiated to high doses. *J. Nucl. Mater* **2016**, *480*, 100–108. [CrossRef]
14. Guo, F.; Li, K.; Huang, X.; Xie, Z.; Gong, F. Understanding the wear failure mechanism of TiAlSiCN nanocomposite coating at evaluated temperatures. *Tribol. Int.* **2021**, *154*, 106716. [CrossRef]
15. Bagdasaryan, A.A.; Pshyk, A.V.; Coy, L.E.; Kempiński, M.; Pogrebnjak, A.D.; Beresnev, V.M.; Jurga, S. Structural and mechanical characterization of (TiZrNbHfTa)N/WN multilayered nitride coatings. *Mater. Lett.* **2018**, *229*, 364–367. [CrossRef]
16. Shen, W.; Tsai, M.; Tsai, K.; Juan, C.; Tsai, C.; Yeh, J.; Chang, Y. Superior oxidation resistance of $(Al_{0.34}Cr_{0.22}Nb_{0.11}Si_{0.11}Ti_{0.22})$ 50N50 high-entropy nitride. *J. Electrochem. Soc.* **2013**, *160*, C531. [CrossRef]
17. Kretschmer, A.; Kirnbauer, A.; Moraes, V.; Primetzhofer, D.; Yalamanchili, K.; Rudigier, H.; Mayrhofer, P.H. Improving phase stability, hardness, and oxidation resistance of reactively magnetron sputtered (Al, Cr, Nb, Ta, Ti) N thin films by Si-alloying. *Surf. Coat. Technol.* **2021**, *416*, 127162. [CrossRef]
18. Lin, M.-I.; Tsai, M.-H.; Shen, W.-J.; Yeh, J.-W. Evolution of structure and properties of multi-component (AlCrTaTiZr)Ox films. *Thin Solid Films* **2010**, *518*, 2732–2737. [CrossRef]
19. Kirnbauer, A.; Spadt, C.; Koller, C.M.; Kolozsvári, S.; Mayrhofer, P.H. High-entropy oxide thin films based on Al–Cr–Nb–Ta–Ti. *Vacuum* **2019**, *168*, 108850. [CrossRef]
20. Cheng, K.-H.; Lai, C.-H.; Lin, S.-J.; Yeh, J.-W. Structural and mechanical properties of multi-element (AlCrMoTaTiZr) Nx coatings by reactive magnetron sputtering. *Thin Solid Films* **2011**, *519*, 3185–3190. [CrossRef]
21. Jhong, Y.-S.; Huang, C.-W.; Lin, S.-J. Effects of CH4 flow ratio on the structure and properties of reactively sputtered (CrNbSiTiZr) Cx coatings. *Mater. Chem. Phys.* **2018**, *210*, 348–352. [CrossRef]
22. Liang, S.-C.; Chang, Z.-C.; Tsai, D.-C.; Lin, Y.-C.; Sung, H.-S.; Deng, M.-J.; Shieu, F.-S. Effects of substrate temperature on the structure and mechanical properties of (TiVCrZrHf) N coatings. *Appl. Surf. Sci.* **2011**, *257*, 7709–7713. [CrossRef]
23. Malinovskis, P.; Fritze, S.; Riekehr, L.; von Fieandt, L.; Cedervall, J.; Rehnlund, D.; Nyholm, L.; Lewin, E.; Jansson, U. Synthesis and characterization of multicomponent (CrNbTaTiW) C films for increased hardness and corrosion resistance. *Mater. Des.* **2018**, *149*, 51–62. [CrossRef]
24. Chen, R.; Cai, Z.; Pu, J.; Lu, Z.; Chen, S.; Zheng, S.; Zeng, C. Effects of nitriding on the microstructure and properties of VAlTiCrMo high-entropy alloy coatings by sputtering technique. *J. Alloys Compd.* **2020**, *827*, 153836. [CrossRef]
25. Von Fieandt, K.; Riekehr, L.; Osinger, B.; Fritze, S.; Lewin, E. Influence of N content on structure and mechanical properties of multi-component Al-Cr-Nb-Y-Zr based thin films by reactive magnetron sputtering. *Surf. Coat. Technol.* **2020**, *389*, 125614. [CrossRef]
26. Khan, N.A.; Akhavan, B.; Zheng, Z.; Liu, H.; Zhou, C.; Zhou, H.; Chang, L.; Wang, Y.; Liu, Y.; Sun, L. Nanostructured $AlCoCrCu_{0.5}FeNi$ high entropy oxide (HEO) thin films fabricated using reactive magnetron sputtering. *Appl. Surf. Sci.* **2021**, *553*, 149491. [CrossRef]
27. Kim, Y.S.; Park, H.J.; Lim, K.S.; Hong, S.H.; Kim, K.B. Structural and mechanical properties of AlCoCrNi high entropy nitride films: Influence of process pressure. *Coating* **2020**, *10*, 10. [CrossRef]

28. Lin, Y.-C.; Hsu, S.-Y.; Song, R.-W.; Lo, W.-L.; Lai, Y.-T.; Tsai, S.-Y.; Duh, J.-G. Improving the hardness of high entropy nitride ($Cr_{0.35}Al_{0.25}Nb_{0.12}Si_{0.08}V_{0.20}$) N coatings via tuning substrate temperature and bias for anti-wear applications. *Surf. Coat. Technol.* **2020**, *403*, 126417. [CrossRef]
29. Shen, W.-J.; Tsai, M.-H.; Chang, Y.-S.; Yeh, J.-W. Effects of substrate bias on the structure and mechanical properties of ($Al_{1.5}CrNb_{0.5}Si_{0.5}Ti$) Nx coatings. *Thin Solid Films* **2012**, *520*, 6183–6188. [CrossRef]
30. Wang, J.-J.; Chang, S.-Y.; Ouyang, F.-Y. Effect of substrate bias on the microstructure and properties of (AlCrSiNbZr) Nx high entropy nitride thin film. *Surf. Coat. Technol.* **2020**, *393*, 125796. [CrossRef]
31. Tian, L.; Feng, Z.; Xiong, W. Microstructure, microhardness, and wear resistance of AlCoCrFeNiTi/Ni60 coating by plasma spraying. *Coatings* **2018**, *8*, 112. [CrossRef]
32. Li, W.; Liu, P.; Liaw, P.K. Microstructures and properties of high-entropy alloy films and coatings: A review. *Mater. Res. Lett.* **2018**, *6*, 199–229. [CrossRef]
33. Sharma, A. High entropy alloy coatings and technology. *Coatings* **2021**, *11*, 372. [CrossRef]
34. Duchaniya, R.K.; Pandel, U.; Rao, P. Coatings based on high entropy alloys: An overview. *Mater. Today Proc.* **2021**, *44*, 4467–4473. [CrossRef]
35. Zelenitsas, K.; Tsakiropoulos, P. Effect of Al, Cr and Ta additions on the oxidation behaviour of Nb–Ti–Si in situ composites at 800 C. *J. Mater. Sci. Eng. A* **2006**, *416*, 269–280. [CrossRef]
36. Kim, B.G.; Kim, G.M.; Kim, C.J. Oxidation behavior of TiAl-X (X = Cr, V, Si, Mo or Nb) intermetallics at elevated temperature. *J. Scr. Metall. Mater.* **1995**, *33*, 1117–1125. [CrossRef]
37. Miracle, D.B.; Miller, J.D.; Senkov, O.N.; Woodward, C.; Uchic, M.D.; Tiley, J. Exploration and development of high entropy alloys for structural applications. *Entropy* **2014**, *16*, 494–525. [CrossRef]
38. Otto, F.; Yang, Y.; Bei, H.; George, E.P. Relative effects of enthalpy and entropy on the phase stability of equiatomic high-entropy alloys. *Acta Mater.* **2013**, *61*, 2628–2638. [CrossRef]
39. Laurent-Brocq, M.; Perrière, L.; Pirès, R.; Champion, Y. From high entropy alloys to diluted multi-component alloys: Range of existence of a solid-solution. *Mater. Des.* **2016**, *103*, 84–89. [CrossRef]
40. Lai, C.-H.; Lin, S.-J.; Yeh, J.-W.; Chang, S.-Y. Preparation and characterization of AlCrTaTiZr multi-element nitride coatings. *Surf. Coat. Technol.* **2006**, *201*, 3275–3280. [CrossRef]
41. Cheng, K.-H.; Weng, C.-H.; Lai, C.-H.; Lin, S.-J. Study on adhesion and wear resistance of multi-element (AlCrTaTiZr)N coatings. *Thin Solid Films* **2009**, *517*, 4989–4993. [CrossRef]
42. Braeckman, B.R.; Misják, F.; Radnóczi, G.; Depla, D. The influence of Ge and In addition on the phase formation of CoCrCuFeNi high-entropy alloy thin films. *Thin Solid Films* **2016**, *616*, 703–710. [CrossRef]
43. Azibi, M.; Saoula, N.; Madaoui, N.; Aknouche, H. Effects of Nitrogen Content on the Structural, Mechanical, and Corrosion Properties of ZrN Thin Films Grown on AISI 316L by Radiofrequency Magnetron Sputtering. *Cryst. Res. Technol.* **2021**, *56*, 2100096. [CrossRef]
44. Shukla, K.; Rane, R.; Alphonsa, J.; Maity, P.; Mukherjee, S. Structural, mechanical and corrosion resistance properties of Ti/TiN bilayers deposited by magnetron sputtering on AISI 316L. *Surf. Coat. Technol.* **2017**, *324*, 167–174. [CrossRef]
45. Ariza, E.; Rocha, L.A.; Vaz, F.; Cunha, L.; Ferreira, S.C.; Carvalho, P.; Rebouta, L.; Alves, E.; Goudeau, P.; Rivière, J.P. Corrosion resistance of ZrNxOy thin films obtained by rf reactive magnetron sputtering. *Thin Solid Films* **2004**, *469-470*, 274–281. [CrossRef]
46. Kozlovskiy, A.; Shlimas, I.; Dukenbayev, K.; Zdorovets, M. Structure and corrosion properties of thin TiO2 films obtained by magnetron sputtering. *Vacuum* **2019**, *164*, 224–232. [CrossRef]
47. Dou, D.; Li, X.; Zheng, Z.; Li, J. Coatings of FeAlCoCuNiV high entropy alloy. *Surf. Eng.* **2016**, *32*, 766–770. [CrossRef]
48. Hsueh, H.-T.; Shen, W.-J.; Tsai, M.-H.; Yeh, J.-W. Effect of nitrogen content and substrate bias on mechanical and corrosion properties of high-entropy films $(AlCrSiTiZr)_{100-x}Nx$. *Surf. Coat. Technol.* **2012**, *206*, 4106–4112. [CrossRef]
49. Schneider, J.M. How high is the entropy in high entropy ceramics? *J. Appl. Phys.* **2021**, *130*, 150903. [CrossRef]
50. Kirnbauer, A.; Kretschmer, A.; Koller, C.; Wojcik, T.; Paneta, V.; Hans, M.; Schneider, J.; Polcik, P.; Mayrhofer, P. Mechanical properties and thermal stability of reactively sputtered multi-principal-metal Hf-Ta-Ti-V-Zr nitrides. *Surf. Coat. Technol.* **2020**, *389*, 125674. [CrossRef]
51. Billard, A.; Perry, F. Pulvérisation cathodique magnétron, Techniques de l'ingénieur. *Matériaux Métalliques* **1762**, *8733*, 2005.
52. Mattox, D.M. Physical vapor deposition (PVD) processes. *Met. Finish.* **2002**, *100*, 394–408. [CrossRef]
53. Manasterski, C. *La Pulvérisation Cathodique Industrielle*; PPUR Presses Polytechniques: Lausanne, Switzerland, 2005.
54. Bishop, C. *Vacuum Deposition onto Webs, Films and Foils*; William Andrew: Norwich, NY, USA, 2011.
55. Michiels, M.; Konstantinidis, S.; Snyders, R. La Pulvérisation Cathodique Magnétron en Régime D'impulsions de Haute Puissance (Hipims). 2013. Available online: https://www.techniques-ingenieur.fr/base-documentaire/innovation-th10/nanomateriaux-synthese-et-elaboration-42195210/la-pulverisation-cathodique-magnetron-en-regime-d-impulsions-de-haute-puissance-hipims-in207/ (accessed on 17 January 2022).
56. Xu, Y.; Li, G.; Li, G.; Gao, F.; Xia, Y. Effect of bias voltage on the growth of super-hard (AlCrTiVZr)N high-entropy alloy nitride films synthesized by high power impulse magnetron sputtering. *Appl. Surf. Sci.* **2021**, *564*, 150417. [CrossRef]
57. Xu, Y.; Li, G.; Xia, Y. Synthesis and characterization of super-hard AlCrTiVZr high-entropy alloy nitride films deposited by HiPIMS. *Appl. Surf. Sci.* **2020**, *523*, 146529. [CrossRef]

58. Bachani, S.K.; Wang, C.-J.; Lou, B.-S.; Chang, L.-C.; Lee, J.-W. Fabrication of TiZrNbTaFeN high-entropy alloys coatings by HiPIMS: Effect of nitrogen flow rate on the microstructural development, mechanical and tribological performance, electrical properties and corrosion characteristics. *J. Alloys Compd.* **2021**, *873*, 159605. [CrossRef]
59. Cui, P.; Li, W.; Liu, P.; Zhang, K.; Ma, F.; Chen, X.; Feng, R.; Liaw, P.K. Effects of nitrogen content on microstructures and mechanical properties of (AlCrTiZrHf) N high-entropy alloy nitride films. *J. Alloys Compd.* **2020**, *834*, 155063. [CrossRef]
60. Ren, B.; Yan, S.; Zhao, R.; Liu, Z. Structure and properties of (AlCrMoNiTi) Nx and (AlCrMoZrTi) Nx films by reactive RF sputtering. *Surf. Coat. Technol.* **2013**, *235*, 764–772. [CrossRef]
61. Chang, C.; Li, P.; Wu, Q.; Wang, M.; Sung, C.; Hsu, C.-Y.J.M.T. Nanostructured and mechanical properties of high-entropy alloy nitride films prepared by magnetron sputtering at different substrate temperatures. *Mater. Technol.* **2019**, *34*, 343–349. [CrossRef]
62. Zhao, F.; Song, Z.; Zhang, G.; Hou, X.; Deng, D. Effects of substrate bias on structure and mechanical properties of AlCrTiWNbTa coatings. *Surf. Eng.* **2013**, *29*, 778–782. [CrossRef]
63. Yu, X.; Wang, J.; Wang, L.; Huang, W. Fabrication and characterization of CrNbSiTiZr high-entropy alloy films by radio-frequency magnetron sputtering via tuning substrate bias. *Surf. Coat. Technol.* **2021**, *412*, 127074. [CrossRef]
64. Wang, J.; Kuang, S.; Yu, X.; Wang, L.; Huang, W. Tribo-mechanical properties of CrNbTiMoZr high-entropy alloy film synthesized by direct current magnetron sputtering. *Surf. Coat. Technol.* **2020**, *403*, 126374. [CrossRef]
65. Dai, C.-d.; Fu, Y.; Guo, J.-x.; Du, C.-w. Effects of substrate temperature and deposition time on the morphology and corrosion resistance of FeCoCrNiMo 0.3 high-entropy alloy coating fabricated by magnetron sputtering. *Int. J. Min. Met. Mater.* **2020**, *27*, 1388–1397. [CrossRef]
66. Sun, X.; Cheng, X.; Cai, H.; Ma, S.; Xu, Z.; Ali, T. Microstructure, mechanical and physical properties of FeCoNiAlMnW high-entropy films deposited by magnetron sputtering. *Appl. Surf. Sci.* **2020**, *507*, 145131. [CrossRef]
67. Behravan, N.; Farhadizadeh, A.; Ghasemi, S.; Khademi, A.; Shojaei, H.; Ghomi, H. The pressure dependence of structure and composition of sputtered AlCrSiTiMoO high entropy thin film. *J. Alloys Compd.* **2021**, *852*, 156421. [CrossRef]
68. Liu, L.; Zhu, J.B.; Hou, C.; Li, J.C.; Jiang, Q. Dense and smooth amorphous films of multicomponent FeCoNiCuVZrAl high-entropy alloy deposited by direct current magnetron sputtering. *Mater. Des.* **2013**, *46*, 675–679. [CrossRef]
69. Zhao, S.; Wu, H.; Yin, R.; Wang, X.; Zhong, H.; Fu, Q.; Wan, W.; Cheng, T.; Shi, Y.; Cai, G. Preparation and electrocatalytic properties of (FeCrCoNiAl$_{0.1}$) Ox high-entropy oxide and NiCo-(FeCrCoNiAl$_{0.1}$) Ox heterojunction films. *J. Alloys Compd.* **2021**, *868*, 159108. [CrossRef]
70. Bi, L.; Li, X.; Li, Z.; Hu, Y.; Zhang, J.; Wang, Q.; Dong, C.; Zheng, Y.; Liaw, P.K. Performance and local structure evolution of NbMoTaWV entropy-stabilized oxide thin films with variable oxygen content. *Surf. Coat. Technol.* **2020**, *402*, 126326. [CrossRef]
71. Li, H.; Jiang, N.; Li, J.; Huang, J.; Kong, J.; Xiong, D. Hard and tough (NbTaMoW) Nx high entropy nitride films with sub-stoichiometric nitrogen. *J. Alloys Compd.* **2021**, *889*, 161713. [CrossRef]
72. Xia, A.; Dedoncker, R.; Glushko, O.; Cordill, M.J.; Depla, D.; Franz, R. Influence of the nitrogen content on the structure and properties of MoNbTaVW high entropy alloy thin films. *J. Alloys Compd.* **2021**, *850*, 156740. [CrossRef]
73. Zhang, C.; Lu, X.; Wang, C.; Sui, X.; Wang, Y.; Zhou, H.; Hao, J. Tailoring the microstructure, mechanical and tribocorrosion performance of (CrNbTiAlV) Nx high-entropy nitride films by controlling nitrogen flow. *J. Mater. Sci. Technol.* **2022**, *107*, 172–182. [CrossRef]
74. Lin, Y.-C.; Hsu, S.-Y.; Lai, Y.-T.; Kuo, P.-H.; Tsai, S.-Y.; Duh, J.-G. Effect of the $N_2/(Ar+ N_2)$ ratio on mechanical properties of high entropy nitride (Cr0.35Al$_{0.25}$Nb$_{0.12}$Si$_{0.08}$V$_{0.20}$) Nx films. *Mater. Chem. Phys.* **2021**, *274*, 125195. [CrossRef]
75. El Garah, M.; Touaibia, D.E.; Achache, S.; Michau, A.; Sviridova, E.; Postnikov, P.S.; Chehimi, M.M.; Schuster, F.; Sanchette, F. Effect of nitrogen content on structural and mechanical properties of AlTiZrTaHf(-N) high entropy films deposited by reactive magnetron sputtering. *Surf. Coat. Technol.* **2022**, *432*, 128051. [CrossRef]
76. Chen, L.; Li, W.; Liu, P.; Zhang, K.; Ma, F.; Chen, X.; Zhou, H.; Liu, X. Microstructure and mechanical properties of (AlCrTiZrV) Nx high-entropy alloy nitride films by reactive magnetron sputtering. *Vacuum* **2020**, *181*, 109706. [CrossRef]
77. Von Fieandt, K.; Paschalidou, E.-M.; Srinath, A.; Soucek, P.; Riekehr, L.; Nyholm, L.; Lewin, E. Multi-component (Al, Cr, Nb, Y, Zr) N thin films by reactive magnetron sputter deposition for increased hardness and corrosion resistance. *Thin Solid Films* **2020**, *693*, 137685. [CrossRef]
78. Khan, N.A.; Akhavan, B.; Zhou, C.; Zhou, H.; Chang, L.; Wang, Y.; Liu, Y.; Bilek, M.M.; Liu, Z. High entropy nitride (HEN) thin films of AlCoCrCu0. 5FeNi deposited by reactive magnetron sputtering. *Surf. Coat. Technol.* **2020**, *402*, 126327. [CrossRef]
79. Xing, Q.; Wang, H.; Chen, M.; Chen, Z.; Li, R.; Jin, P.; Zhang, Y. Mechanical properties and corrosion resistance of NbTiAlSiZrNx high-entropy films prepared by RF magnetron sputtering. *Entropy* **2019**, *21*, 396. [CrossRef]
80. Zhang, Y.; Yan, X.-H.; Liao, W.-B.; Zhao, K. Effects of nitrogen content on the structure and mechanical properties of (Al0. 5CrFeNiTi0. 25) Nx high-entropy films by reactive sputtering. *Entropy* **2018**, *20*, 624. [CrossRef]
81. Feng, X.; Tang, G.; Ma, X.; Sun, M.; Wang, L. Characteristics of multi-element (ZrTaNbTiW) N films prepared by magnetron sputtering and plasma based ion implantation. *Nucl. Instrum. Methods Phys. Res. B* **2013**, *301*, 29–35. [CrossRef]
82. Ren, B.; Lv, S.; Zhao, R.; Liu, Z.; Guan, S. Effect of sputtering parameters on (AlCrMnMoNiZr) N films. *Surf. Eng.* **2014**, *30*, 152–158. [CrossRef]
83. Braic, V.; Vladescu, A.; Balaceanu, M.; Luculescu, C.; Braic, M. Nanostructured multi-element (TiZrNbHfTa) N and (TiZrNbHfTa) C hard coatings. *Surf. Coat. Technol.* **2012**, *211*, 117–121. [CrossRef]

84. Tsai, C.-W.; Lai, S.-W.; Cheng, K.-H.; Tsai, M.-H.; Davison, A.; Tsau, C.-H.; Yeh, J.-W.J.T.S.F. Strong amorphization of high-entropy AlBCrSiTi nitride film. *Thin Solid Films* **2012**, *520*, 2613–2618. [CrossRef]
85. Khan, N.A.; Akhavan, B.; Zhou, H.; Chang, L.; Wang, Y.; Sun, L.; Bilek, M.M.; Liu, Z. High entropy alloy thin films of $AlCoCrCu_{0.5}FeNi$ with controlled microstructure. *Appl. Surf. Sci.* **2019**, *495*, 143560. [CrossRef]
86. Shaginyan, L.; Krapivka, N.; Firstov, S.; Kopylov, I. Properties of coatings of the Al–Cr–Fe–Co–Ni–Cu–V high entropy alloy produced by the magnetron sputtering. *J. Superhard Mater.* **2016**, *38*, 25–33. [CrossRef]
87. Kao, W.; Su, Y.; Horng, J.; Wu, H. Effects of carbon doping on mechanical, tribological, structural, anti-corrosion and anti-glass-sticking properties of CrNbSiTaZr high entropy alloy coatings. *Thin Solid Films* **2021**, *717*, 138448. [CrossRef]
88. Hsieh, M.-H.; Tsai, M.-H.; Shen, W.-J.; Yeh, J.-W. Structure and properties of two Al–Cr–Nb–Si–Ti high-entropy nitride coatings. *Surf. Coat. Technol.* **2013**, *221*, 118–123. [CrossRef]
89. Kuang, S.; Wang, J.; Wang, L.; Huang, W.; Zhou, Z. Improvement of the mechanical and the tribological properties of CrNbTiMoZr coatings through the incorporation of carbon and the adjustment of the substrate bias voltage. *Surf. Coat. Technol.* **2021**, *412*, 127064. [CrossRef]
90. Cui, Y.; Shen, J.; Manladan, S.M.; Geng, K.; Hu, S. Wear resistance of FeCoCrNiMnAlx high-entropy alloy coatings at high temperature. *Appl. Surf. Sci.* **2020**, *512*, 145736. [CrossRef]
91. Lo, W.-L.; Hsu, S.-Y.; Lin, Y.-C.; Tsai, S.-Y.; Lai, Y.-T.; Duh, J.-G. Improvement of high entropy alloy nitride coatings (AlCrNbSiTiMo) N on mechanical and high temperature tribological properties by tuning substrate bias. *Surf. Coat. Technol.* **2020**, *401*, 126247. [CrossRef]
92. Bachani, S.K.; Wang, C.-J.; Lou, B.-S.; Chang, L.-C.; Lee, J.-W. Microstructural characterization, mechanical property and corrosion behavior of VNbMoTaWAl refractory high entropy alloy coatings: Effect of Al content. *Surf. Coat. Technol.* **2020**, *403*, 126351. [CrossRef]
93. Hung, S.-B.; Wang, C.-J.; Chen, Y.-Y.; Lee, J.-W.; Li, C.-L. Thermal and corrosion properties of V-Nb-Mo-Ta-W and V-Nb-Mo-Ta-W-Cr-B high entropy alloy coatings. *Surf. Coat. Technol.* **2019**, *375*, 802–809. [CrossRef]
94. Wang, H.-d.; Liu, J.-n.; Xing, Z.-g.; Ma, G.-Z.; Cui, X.-f.; Jin, G.; Xu, B.-s. Microstructure and corrosion behaviour of AlCoFeNiTiZr high-entropy alloy films. *Surf. Eng.* **2020**, *36*, 78–85. [CrossRef]
95. Feng, X.; Tang, G.; Gu, L.; Ma, X.; Sun, M.; Wang, L. Preparation and characterization of TaNbTiW multi-element alloy films. *Appl. Surf. Sci.* **2012**, *261*, 447–453. [CrossRef]
96. Tsai, D.-C.; Deng, M.-J.; Chang, Z.-C.; Kuo, B.-H.; Chen, E.-C.; Chang, S.-Y.; Shieu, F.-S. Oxidation resistance and characterization of (AlCrMoTaTi)-Six-N coating deposited via magnetron sputtering. *J. Alloys Compd.* **2015**, *647*, 179–188. [CrossRef]
97. Hruška, P.; Lukáč, F.; Cichoň, S.; Vondráček, M.; Čížek, J.; Fekete, L.; Lančok, J.; Veselý, J.; Minárik, P.; Cieslar, M. Oxidation of amorphous HfNbTaTiZr high entropy alloy thin films prepared by DC magnetron sputtering. *J. Alloys Compd.* **2021**, *869*, 157978. [CrossRef]
98. Kirnbauer, A.; Wagner, A.; Moraes, V.; Primetzhofer, D.; Hans, M.; Schneider, J.; Polcik, P.; Mayrhofer, P. Thermal stability and mechanical properties of sputtered (Hf, Ta, V, W, Zr)-diborides. *Acta Mater.* **2020**, *200*, 559–569. [CrossRef]
99. Cemin, F.; Jimenez, M.J.; Leidens, L.M.; Figueroa, C.A.; Alvarez, F. A thermodynamic study on phase formation and thermal stability of AlSiTaTiZr high-entropy alloy thin films. *J. Alloys Compd.* **2020**, *838*, 155580. [CrossRef]
100. Braic, V.; Balaceanu, M.; Braic, M.; Vladescu, A.; Panseri, S.; Russo, A. Characterization of multi-principal-element (TiZrNbHfTa) N and (TiZrNbHfTa) C coatings for biomedical applications. *J. Mech. Behav. Biomed. Mater.* **2012**, *10*, 197–205. [CrossRef] [PubMed]
101. Vladescu, A.; Titorencu, I.; Dekhtyar, Y.; Jinga, V.; Pruna, V.; Balaceanu, M.; Dinu, M.; Pana, I.; Vendina, V.; Braic, M. In vitro biocompatibility of Si alloyed multi-principal element carbide coatings. *PLoS ONE* **2016**, *11*, e0161151. [CrossRef] [PubMed]
102. Codescu, M.M.; Vladescu, A.; Geanta, V.; Voiculescu, I.; Pana, I.; Dinu, M.; Kiss, A.E.; Braic, V.; Patroi, D.; Marinescu, V.E.; et al. Zn based hydroxyapatite based coatings deposited on a novel FeMoTaTiZr high entropy alloy used for bone implants. *Surf. Interfaces* **2021**, *28*, 101591. [CrossRef]
103. Peng, X.; Chen, L. Effect of high entropy alloys TiVCrZrHf barrier layer on microstructure and texture of Cu thin films. *Mater. Lett.* **2018**, *230*, 5–8. [CrossRef]
104. Li, R.; Qiao, B.; Shang, H.; Zhang, J.; Jiang, C.; Zhang, W. Multi-component AlCrTaTiZrMo-nitride film with high diffusion resistance in copper metallization. *J. Alloys Compd.* **2018**, *748*, 258–264. [CrossRef]
105. Lu, X.; Zhang, C.; Wang, C.; Cao, X.; Ma, R.; Sui, X.; Hao, J.; Liu, W. Investigation of (CrAlTiNbV) Nx high-entropy nitride coatings via tailoring nitrogen flow rate for anti-wear applications in aviation lubricant. *Appl. Surf. Sci.* **2021**, *557*, 149813. [CrossRef]
106. Shen, W.-J.; Tsai, M.-H.; Yeh, J.-W. Machining performance of sputter-deposited $(Al_{0.34}Cr_{0.22}Nb_{0.11}Si_{0.11}Ti_{0.22})_{50}N_{50}$ high-entropy nitride coatings. *Coatings* **2015**, *5*, 312–325. [CrossRef]